

Thermal-neutron scattering lengths and capture by even calcium isotopes

S. Raman, S. Kahane,* R. M. Moon, and J. A. Fernandez-Baca
Oak Ridge National Laboratory, Oak Ridge, Tennessee 37831

J. L. Zarestky
Ames Laboratory, Iowa State University, Ames, Iowa 50011

J. E. Lynn[†] and J. W. Richardson, Jr.
Argonne National Laboratory, Argonne, Illinois 60439
(Received 5 December 1988)

Neutron-diffraction patterns have been measured for isotopically enriched powder samples of calcite using both steady-state and pulsed-neutron techniques. Greatly enhanced precision over previous work has been achieved for ^{40}Ca and ^{44}Ca , while the results for ^{42}Ca , ^{43}Ca , and ^{48}Ca represent new data. The coherent scattering lengths deduced from these measurements have been employed in a more definitive analysis of primary electric-dipole gamma rays from thermal-neutron capture. In three cases (^{40}Ca , ^{42}Ca , and ^{48}Ca) the estimates from a spherical optical-model formulation of the direct-capture mechanism are in agreement with the experimental cross sections. In ^{44}Ca the theory overestimates the measured cross sections on average by about 60%; this divergence can be explained by considering the modifications to the theory due to collective vibrations of the ^{44}Ca core.

I. INTRODUCTION

In a recent paper¹ the cross sections of the primary electric-dipole gamma rays from slow-neutron capture by the even calcium isotopes were analyzed to establish the importance of the direct-capture mechanism in this group of nuclides. Earlier quantitative work^{2,3} had established the predominance of this mechanism, based on the original channel-capture theory⁴ and fully developed into an optical-model formulation in Refs. 2, 5, and 6, for other groups of light nuclides. In the calcium isotopes, too, very strong indications of the major role of the direct mechanism were found. However, a key parameter required for the calculation of the direct-capture cross section is the thermal-neutron coherent scattering length (or, for odd-mass nuclides, the spin-dependent scattering lengths). In the case of calcium this quantity was known for only two of the five isotopes studied—and then not very accurately. Thus, the analysis was not nearly as definitive as the rather complete body of data on the capture cross sections, spectra, and the final-state spectroscopic factors would otherwise have allowed. We have therefore undertaken measurements of the coherent scattering lengths (also referred to here and in the literature as scattering amplitudes) of most of the stable isotopes of calcium, with the aims of determining these quantities where previously unknown and of greatly improving the accuracy of the two known values. Armed with this knowledge we can proceed to a revised and more definitive analysis of the capture data.

Direct experimental values are available for the coherent scattering amplitudes b of almost all the naturally occurring isotopes of the light elements ($Z < 30$). A notable exception is the case of calcium which has six isotopes. Two of these were measured by Shull and Wollan⁷

in early neutron-diffraction experiments. They obtained for ^{40}Ca , $b_{40} = 4.9$ fm, and for ^{44}Ca , $b_{44} = 1.8$ fm, with experimental errors estimated to be 3–4%. These are the only reported direct measurements on separated calcium isotopes. Several values for the coherent amplitude of natural calcium have been reported. Based on diffraction measurements Shull and Wollan⁷ gave 4.9 fm, Atogi⁸ gave 4.88(7) fm, and Kvik *et al.*⁹ gave 4.65(3) fm. In a 1977 survey of available data, Koester¹⁰ recommended 4.90(3) fm, but more recent Christiansen filter measurements by Koester¹¹ gave 4.71(3) fm. In unpublished diffraction experiments on calcite, Richardson¹² found 4.745(23) fm.

II. COHERENT SCATTERING MEASUREMENTS

A. Experimental details

Six isotopically enriched samples of CaCO_3 powder were borrowed from the Isotopes Section of the Oak Ridge National Laboratory in 5-g amounts. A natural calcium sample was also measured using reagent-grade CaCO_3 (Mallinckrodt 4072). The isotopic compositions of these samples are shown in Table I. The natural abundance of ^{46}Ca is only 0.003%; its contribution is negligibly small in all the samples.

Two series of experiments were performed. All the samples, except the one designated 43-2, were measured on the Ames Laboratory triple-axis spectrometer at the Oak Ridge Research Reactor (ORR). A supplementary series of experiments on samples designated as natural, 44, and 43-2, were performed at the Intense Pulsed Neutron Source (IPNS) at the Argonne National Laboratory.

For the ORR experiments, the samples were loaded into a cylindrical aluminum cell, and the spectrometer

TABLE I. Isotopic composition (in %) of calcium in various calcite samples.

Sample	Batch No.	^{40}Ca	^{42}Ca	^{43}Ca	^{44}Ca	^{48}Ca
natural		96.96	0.64	0.15	2.06	0.19
40	107 701	99.97	0.01		0.02	
42	139 690	4.96	94.42	0.06	0.56	
43-1	169 101	10.36	0.80	83.73	5.11	
43-2	139 701	12.78	0.65	81.12	5.40	0.05
44	136 401	1.26	0.08	0.06	98.60	
48	192 926	2.59	0.03	0.01	0.10	97.27

was set for elastic scattering with a wavelength of 2.344 Å. The collimation before and after the sample was 40 min, and there was an 80-min collimator after the analyzer. Pyrolytic graphite was used as monochromator, analyzer, and $\lambda/2$ filter. Data were collected at room temperature for the first nine peaks in the calcite pattern.

For the IPNS experiments, vanadium sample cells were used on the general purpose powder diffractometer. Data at room temperature were collected over a much broader range of momentum transfer, with data from $d=2.87$ to 0.44 Å included in the analysis. The standard IPNS profile refinement program for time-of-flight neutron-powder-diffraction data was used in the analyses.

B. Results

Calcite, one of the polymorphic forms of CaCO_3 , has a rhombohedral structure with space group $R\bar{3}c$. We have used a hexagonal cell to describe this structure with $a=4.9896$ and $c=17.061$ Å. In this cell are six molecules of CaCO_3 with only one variable position parameter that determines the oxygen positions. The ORR diffraction patterns are shown in Figs. 1 and 2. The pronounced changes in these patterns are due solely to the change in the average nuclear scattering amplitude for calcium in the different samples. The pattern for the natural calci-

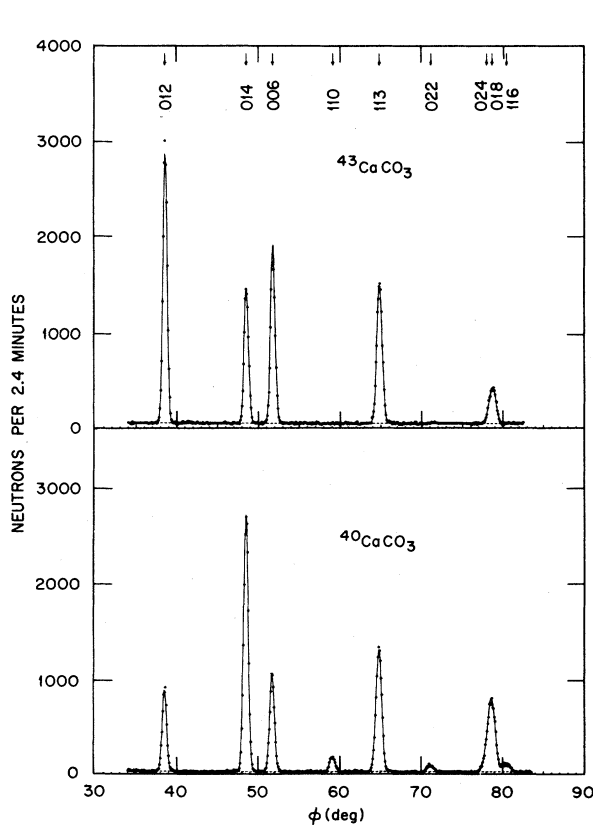


FIG. 1. Neutron-diffraction patterns for the samples designated as 40 and 43-1 in Table I. The aluminum peaks from the sample holder and the impurity peaks in sample 43-1 have been deleted. The angle $\phi=(2\theta+3.12)$ deg, where 2θ is the scattering angle.

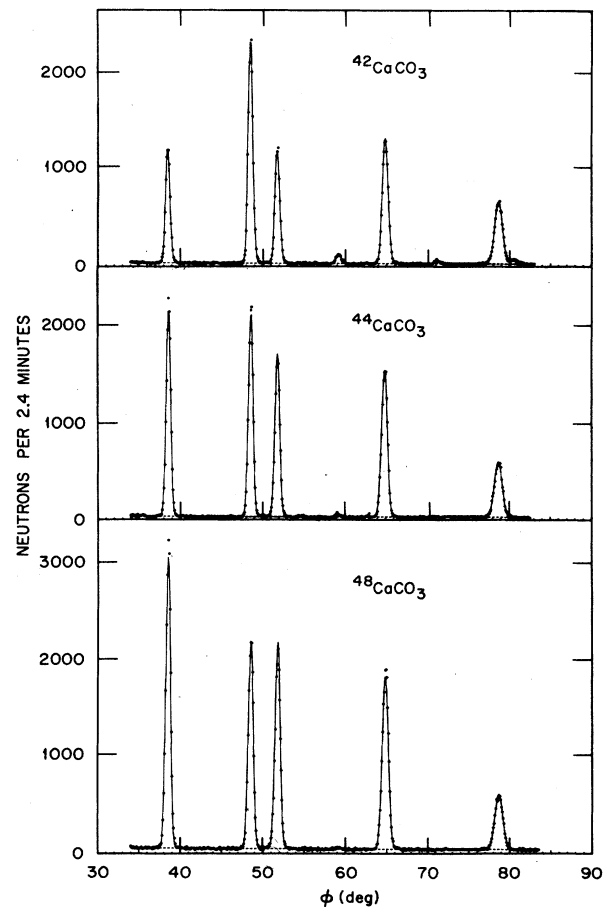


FIG. 2. Neutron-diffraction patterns for the samples designated as 42, 44, and 48 in Table I.

um sample is not shown because it is nearly identical to that for the ^{40}Ca sample. With one exception, none of the samples showed any impurity peaks. The 43-1 pattern had two weak peaks which could be indexed as (002) and (111) of vaterite,¹³ an orthorhombic form of CaCO_3 . However, the observed and calculated intensity ratios are in very poor agreement; consequently the origin of these peaks should be considered unknown. From the scale factor needed to fit the calcite peaks in the 43-1 sample, it was concluded that 7% of the sample did not contribute to the calcite peaks.

Integrated intensities were obtained by numerical integration and by fitting Gaussian peak shapes to the data, with excellent agreement between these two methods. One pair of peaks, the (024) and (018), were not resolved; thus there were eight independent intensities observed. The integrated intensity for a particular peak is given by

$$I_{\text{calc}} = K \frac{jF^2 e^{-G\alpha^2}}{\sin\theta \sin 2\theta}, \quad (1)$$

where j is the number of equivalent reflections, F is the structure factor, $\exp(-G\alpha^2)$ is a preferred orientation correction factor as given by Rietveld,¹⁴ and 2θ is the scattering angle. The scale factor K is

$$K = CN_c^2 A \rho' / \rho, \quad (2)$$

where C is a sample-independent calibration factor for a particular experimental arrangement, N_c is the number of unit cells per unit volume, A is the absorption factor (independent of scattering angle for our calcite samples), and ρ'/ρ is the packing fraction for a powder sample. The scale factor K is a constant for all the peaks in a given pattern. The structure factor is

$$F = \sum_j b_j \exp[2\pi i(hx_{1j} + kx_{2j} + lx_{3j})] \times T(h, k, l, U_{11j}, U_{33j}, U_{12j}, U_{13j}), \quad (3)$$

where the x_{ij} are fractional coordinates of an atom with nuclear scattering amplitude b_j , T is the anisotropic temperature factor, and the sum goes over all the atoms in the unit cell. The positions and the U parameters are known from the work of Effenberger *et al.*,¹⁵ who did a

structural refinement based on x-ray diffraction by single crystals. The nuclear scattering amplitudes of carbon and oxygen were taken to be 6.648(1) and 5.805(5) fm, respectively.¹⁰ In the preferred orientation factor [see Eq. (1)], α is the angle between the scattering vector and the hexagonal C axis, and G is an adjustable parameter.

Least-squares fits of Eq. (1) to the eight observed intensities were performed with three adjustable parameters: the scale factor, the calcium-scattering amplitude, and the preferred orientation parameter G . The parameter G was always quite small (it averaged to -0.01 for the six samples) and therefore was set equal to zero for the final analysis.

The results of this analysis are shown in Table II. The first column represents a check on the consistency of the results relative to a standard nickel sample. Measured packing densities and transmissions were used to determine ρ'/ρ and A in Eq. (2). From the fitted scale factors, the calibration constant C was determined for each sample, and the quantity S in Table II is the ratio of C for each sample to C_{Ni} . The values of S should all be unity, within the experimental error. The failure of this test for the case of 43-1 has already been noted. The calibration constant depends linearly on the volume of sample in the beam, hence the conclusion that the impurity phase in 43-1 was 7% of the total. The presence of an unknown phase in this case should not affect the determination of \bar{b}_{Ca} , provided that the unknown phase makes negligible contributions to the calcite peaks. The R factor in Table II is a measure of the goodness of fit. The Rietveld profile analysis technique¹⁴ has also been applied to these data, resulting in excellent agreement with the integrated intensity analysis. The solid lines of Figs. 1 and 2 come from the profile analysis fits.

The small uncertainty related to the impurity peaks in the 43-1 sample was the prime motivation for the series of experiments as IPNS. Another sample (43-2) enriched in ^{43}Ca was obtained for this purpose. Also, as a check on the consistency of the two experimental techniques, the samples designated natural and 44 were repeated at the IPNS. In the profile refinement of these data, a total of 23 parameters were refined: a scale factor, the oxygen position parameter, nine thermal parameters, three peak

TABLE II. Summary of results obtained by fitting calcite structure to observed intensities. In our notation $0.99(2) = 0.99 \pm 0.02$, etc.

Sample	S^a	Oak Ridge Research Reactor		Argonne Intense Pulse Neutron Source		Final \bar{b}_{Ca} (fm)
		\bar{b}_{Ca} (fm)	R^b	\bar{b}_{Ca} (fm)	R^b	
natural	0.99(2)	4.71(7)	1.8	4.60(2)	7.4	4.66(5)
40	1.00(2)	4.68(7)	1.7			4.68(7)
42	0.99(2)	3.41(8)	2.6			3.41(8)
43-1	0.93(2)	-0.60(11)	2.7			-0.60(11)
43-2				-0.63(8)	9.2	-0.63(8)
44	1.01(2)	1.43(7)	2.0	1.50(3)	8.2	1.46(5)
48	0.97(2)	0.47(8)	2.0			0.47(8)

^aThe factor S is the ratio of the absolute calibration constant, obtained from the fitted scale factor, to the same quantity obtained from results for a standard nickel sample.

^bBy definition, $R = 100(\sum |I_{\text{obs}} - I_{\text{calc}}| / \sum I_{\text{obs}})$, where the summation goes over all the independent observations.

TABLE III. Bound (b) and free nuclear (a) coherent neutron scattering lengths for calcium isotopes.

Isotope	Ref. 7 b (fm)	This work b (fm)	This work a (fm) ^a
⁴⁰ Ca	4.9±0.2	4.73±0.05	4.64
⁴² Ca		3.36±0.10	3.31
⁴³ Ca		-1.56±0.09	-1.50
⁴⁴ Ca	1.8±0.1	1.42±0.06	1.41
⁴⁸ Ca		0.36±0.09	0.38

^aDeduced from $a = [A/(A+1)](b+0.00138Z)$ given by Mughabghab, Divadeenam, and Holden, Ref. 18. These a values are carried over to Table IV and listed there as $a(X)$.

shape parameters, two lattice parameters, five background parameters, one absorption parameter, and the calcium-scattering amplitude. The lattice parameters and the oxygen-position parameter were in good agreement with accepted values. For the natural calcium sample, the nine thermal parameters were in good agreement with those of Effenberger *et al.*¹⁵ used in the analysis of the ORR data; the agreement was not as good for the two isotopically enriched samples. Fortunately, the best value for the calcium amplitude was not very sensitive to values for the other parameters.

As seen in Table II, satisfactory agreement was obtained between the ORR and IPNS experiments. In addition, the sample 43-2 did not show any impurity peaks. An absolute calibration procedure was not used for the IPNS experiments; therefore, the arbitrary scale factors are omitted in Table II. For the final result the ORR and IPNS duplicate data were assigned equal weights with the final uncertainty based on that of the ORR result. These seven final values of \bar{b} for the different samples, given in the last column of Table II, were used as input to a least-squares fit of

$$\bar{b}_i = \sum_{j=1}^5 C_{ij} b_j, \quad (4)$$

where the C_{ij} are the concentrations given in Table I, and the b_j are the five isotopic scattering amplitudes. The isotopic scattering amplitudes determined in this manner are given in Table III together with the results of Shull and Wollan.⁷

III. ANALYSIS OF CAPTURE DATA WITH SPHERICAL OPTICAL MODEL

A. General remarks

Our analysis of the thermal-neutron-capture γ -ray data proceeds along the same lines as described in Ref. 1. As in that work our choice of global optical model is based on the work of Moldauer;¹⁶ the real well is of Woods-Saxon form with depth $\mathcal{V}_0 = -46$ MeV, potential radius $R = (1.16A^{1/3} + 0.6)$ fm, surface diffuseness parameter $d = 0.62$ fm, while the imaginary potential is a surface term of Gaussian form about the potential radius with spreading width $b = 0.7$ fm and peak strength -15 MeV. For the final p -wave single-particle state, a similar

diffuseness and potential radius were used, but the well depth was adjusted to place the eigenvalue at the binding energy of the final state under study. As in Ref. 1 direct-capture cross sections were calculated by both the global plus valency method ($G+V$) and the specialized optical-model method (S). In the former the coherent scattering length was reproduced by adding a local-level term to the potential scattering length a_{pot} , and a corresponding valence term was added to the potential-capture amplitude to obtain the direct-capture cross section. In the latter (S) method one of the optical-model parameters (well depth, diffuseness, or imaginary potential magnitude) was varied within physically reasonable limits to give a potential scattering length equal to the observed coherent scattering length; the potential-capture cross section $\sigma_{\text{pot},\gamma}$ was then the required direct-capture cross section $\sigma_{\text{dir},\gamma}$. In this, as in previous work, the two methods, when they could be used, gave rather similar results.

As in Ref. 1 (where all quantities used here are further defined) hypothetical compound nucleus capture cross sections $\sigma_{\text{CN},\gamma}$ can be extracted using the formula

$$\sigma_\gamma(X) = (\sigma_{\text{dir},\gamma}^{1/2} \pm \sigma_{\text{CN},\gamma}^{1/2})^2, \quad (5)$$

where $\sigma_\gamma(X)$ is the experimentally measured cross section. The extracted cross section can be translated into a relation for the compound nucleus radiation width if it is assumed that the discrepancy between the potential scattering length of the global optical model and the coherent scattering length is due to the single capturing resonance level. This latter assumption is expressed as

$$R\gamma_{\lambda n}^2/E_\lambda = \Gamma_{\lambda n}/2kE_\lambda \approx R\mathcal{R}^{\text{loc}}, \quad (6)$$

where \mathcal{R}^{loc} is the residual R function for the local levels and is obtained from

$$R\mathcal{R}^{\text{loc}} = a_{\text{pot}} - a_{\text{coh}}. \quad (7)$$

The radiation width relation is then

$$\frac{\langle \Gamma_{\lambda\gamma,\text{CN}}/E_\lambda^3 \rangle}{E_\lambda} \approx \frac{k \langle \sigma_{\text{CN},\gamma}/E_\lambda^3 \rangle}{2\pi R\mathcal{R}^{\text{loc}}}, \quad (8)$$

where k is the neutron wave number.

B. ⁴⁰Ca(n,γ)⁴¹Ca

The revised calculations, along with the experimental data, for this reaction are shown in Table IV(A). From the last column the average value of $\langle \sigma_{\text{CN},\gamma}/E_\lambda^3 \rangle$ is found to be 0.022 mb/MeV. This is to be compared with the value of 0.027 found in Ref. 1 and gives the value $\langle \Gamma_{\lambda\gamma,\text{CN}}/E_\lambda^3 \rangle/E_\lambda = -5.3 \times 10^{-9}$ MeV⁻³. Comparison with the Cameron¹⁷ semiempirical relation for slow neutron partial radiation widths indicates $E_\lambda = -0.7D$ and $\gamma_{\lambda n}^2 = 0.11D$, where D is the s -wave compound level spacing. These are plausible values which support the starting hypothesis that the rather small differences between the experimental and theoretical direct-capture cross sections can be attributed to a small admixture of compound-nucleus amplitude.

C. $^{42}\text{Ca}(n,\gamma)^{43}\text{Ca}$

The coherent scattering length was unknown prior to this study. In Ref. 1 the direct-capture cross section was calculated for a range of values of scattering length. The scattering length that "best fit" the capture was found to be $a=3.4$ fm. The newly measured value $a_{\text{coh}}=3.31$ fm is very close to this and vindicates the conclusion of Ref. 1 that this thermal-neutron reaction represents almost pure direct capture. The analysis is presented in Table IV (B).

An analysis of the residual-capture cross sections as compound-nucleus capture gives $\langle \Gamma_{\lambda\gamma,\text{CN}}/E_\gamma^3 \rangle / E_\lambda = -1.24 \times 10^{-9} \text{ MeV}^{-3}$, indicating (from Cameron's formula) that $E_\lambda = -3D$. This large value indicates also a large reduced neutron width ($\gamma_{\lambda n}^2 = 0.7D$), but this is only a few times larger than the expected mean value.

D. $^{48}\text{Ca}(n,\gamma)^{49}\text{Ca}$

In Ref. 1 a value of the thermal-neutron coherent scattering length ($a = +1.95$ or -1.12 fm) was extrapo-

TABLE IV. Direct capture cross sections for primary $E1$ transitions in the (n,γ) reaction on calcium isotopes. Columns 1, 2, and 3 give the energy, J^π value, and the (d,p) spectroscopic strength of the final state. Column 4 is the primary transition energy (essentially the binding energy of the final state). Column 5 is the average valency capture width and column 6 the potential capture cross section, both calculated using a global optical potential. The entries in column 5 do not include the spin-coupling factor and the spectroscopic factor; those in column 6 do. Column 7 is the calculated cross section using the global plus valence $[G+V]$ procedure. Column 8 contains the calculated cross sections from the specialized optical-model procedure $[S]$. The experimentally determined cross sections are given in column 9. Finally, column 10 gives the minimum hypothesized compound-nucleus cross sections deduced from the differences between column 7 and column 9. In the table subheadings, $a(x)$ refers to the experimental scattering length, while $a(G)$ and $\bar{\Gamma}_n^0/D$ refer to the scattering length and the neutron strength function, respectively, both calculated using the global optical potential.

E_f (MeV)	J_f^π	(d,p) $(2J_f+1)S$	E_γ (MeV)	$(\Gamma_{\gamma,\text{val}}/DE_\gamma^3)$ $\times 10^7$ (MeV $^{-3}$)	$\sigma_{\text{pot},\gamma}$ (mb)	$\sigma_{\text{dir},\gamma}[G+V]$ (mb)	$\sigma_{\text{dir},\gamma}[S]$ (mb)	$\sigma_\gamma[X]$ (mb)	$\sigma_{\text{CN},\gamma}$ (mb)
(A) $^{40}\text{Ca}(n,\gamma)^{41}\text{Ca}$ reaction; $a(X)=4.64$ fm; $a(G)=2.52$ fm; $\bar{\Gamma}_n^0/D=1.87 \times 10^{-4}$									
1.943	$\frac{3}{2}^-$	2.53	6.421	0.615	647	197	205	167±25	1.2
2.462	$\frac{3}{2}^-$	0.90	5.901	0.690	210	66	68	31±5	6.5
3.614	$\frac{1}{2}^-$	0.22	4.750	0.755	34	12	12	9±2	0.2
3.944	$\frac{1}{2}^-$	1.09	4.419	0.835	155	56	58	86±13	3.2
4.603	$\frac{3}{2}^-$	0.15	3.760	1.228	21	8	8	13±3	0.6
4.753	$\frac{1}{2}^-$	0.35	3.611	1.094	40	16	16	30±5	2.2
(B) $^{42}\text{Ca}(n,\gamma)^{43}\text{Ca}$ reaction; $a(X)=3.31$ fm; $a(G)=2.25$ fm; $\bar{\Gamma}_n^0/D=2.70 \times 10^{-4}$									
0.593	$\frac{3}{2}^-$	0.30	7.340	0.685	95	58	51	48±8	0.47
2.046	$\frac{3}{2}^-$	2.73	5.886	0.931	673	426	387	393±60	0.67
2.611	$\frac{1}{2}^-$	0.27	5.322	0.860	49	32	29	37±6	0.18
2.878	$\frac{1}{2}^-$	0.19	5.055	0.928	33	21	19	18±3	0.12
2.943	$\frac{3}{2}^-$	0.20	4.990	1.157	41	26	24	28±4	0.04
3.286	$\frac{3}{2}^-$	0.13	4.647	1.266	24	16	15	21±5	0.34
3.572	$\frac{3}{2}^-$	0.16	4.360	1.371	28	18	17	25±4	0.57
4.207	$\frac{1}{2}^-$	0.85	3.726	1.406	104	70	65	65±10	0.09
(C) $^{44}\text{Ca}(n,\gamma)^{45}\text{Ca}$ reaction; $a(X)=1.41$ fm; $a(G)=2.18$ fm; $\bar{\Gamma}_n^0/D=3.87 \times 10^{-4}$									
1.435	$\frac{3}{2}^-$	0.43	5.980	1.232	106	139	146	95±10	4.2
1.900	$\frac{3}{2}^-$	2.35	5.515	1.370	524	686	723	460±46	22.5
2.249	$\frac{1}{2}^-$	0.35	5.166	1.219	61	79	85	85±10	0.1
2.842	$\frac{3}{2}^-$	0.40	4.573	1.736	71	92	98	35±5	13.5
3.241	$\frac{3}{2}^-$	0.13	4.173	1.941	21	26	28	21±4	0.3
3.418	$\frac{1}{2}^-$	0.68	3.996	1.727	88	112	122	95±10	0.7
3.783	$\frac{3}{2}^-$	0.11	3.632	2.290	15	19	20	8±3	2.3
	$\frac{1}{2}^-$			1.953	13	16	18		1.4
3.838	$(\frac{1}{2})^-$	0.24	3.577	1.991	27	35	38	14±3	4.7
4.616	$\frac{1}{2}^-$	0.40	2.799	2.695	34	42	47	31±5	0.8
5.000	$(\frac{1}{2})^-$	0.47	2.415	3.210	33	41	45	16±4	5.8
(D) $^{48}\text{Ca}(n,\gamma)^{49}\text{Ca}$ reaction; $a(X)=0.38$ fm; $a(G)=3.38$ fm; $\bar{\Gamma}_n^0/D=6.35 \times 10^{-4}$									
0.0	$\frac{3}{2}^-$	3.56	5.147	2.205	401	1169	1186	818±110	31.2
2.023	$\frac{1}{2}^-$	2.06	3.123	3.449	117	294	312	272±40	0.4

lated from an analysis of the total cross-section data made at much higher energies. Our measurement ($a = +0.38$ fm) differs substantially from that extrapolated value; consequently, the new analysis of the capture data is quite different [see Table IV (D)]. There is now close agreement between observation and calculation for the 3.123-MeV transition, but the 5.147-MeV transition is now overestimated by more than three standard deviations. An analysis of the discrepancy in terms of compound-nucleus admixture gives $\langle \sigma_{\text{CN},\gamma}/E_\gamma^3 \rangle = (0.12 \pm 0.06) \text{ mb MeV}^{-3}$ and, hence, $\langle \Gamma_{\lambda\gamma, \text{CN}}/E_\gamma^3 \rangle / E_\lambda = (22 \pm 11) \times 10^{-9} \text{ MeV}^{-3}$. By comparison with the Cameron relation, this result implies a resonance in the region of ≈ 60 keV (for $D = 500$ keV), and the value of $R\mathcal{R}^{\text{loc}} = 3.0$ fm further implies that this resonance has a substantial neutron width of ≈ 16 keV. Such a resonance has not been observed in the measured total cross section above 30 keV. The uncertainties in the deduction of the compound-nucleus component are large and are further compounded by the effect of the Porter-Thomas distribution on such a small sample. Thus, any residual compound nucleus effect is, in reality, probably rather weak. This conclusion is also demanded by the high single-particle purity of the final states, as indicated by their (d, p) spectroscopic factors [see Table IV (D)].

E. $^{44}\text{Ca}(n, \gamma)^{45}\text{Ca}$

Our new measurement of the coherent scattering length ($a = 1.41$ fm) of this nucleus gives a rather different value from the previously used one ($a = 1.8$ fm). Consequently, the estimates of direct-capture cross sections [see Table IV (C)] are changed somewhat from those of Ref. 1. The discrepancies between theory and experiment are greater, and the resulting hypothetical values of compound-nucleus capture are about twice as great as those in Ref. 1. Thus, $\langle \sigma_{\text{CN},\gamma}/E_\gamma^3 \rangle = 0.09 \text{ mb MeV}^{-3}$, implying that $\langle \Gamma_{\lambda\gamma, \text{CN}}/E_\gamma^3 \rangle / E_\lambda = 64 \times 10^{-9} \text{ MeV}^{-3}$. This is 15 times greater than the Cameron estimate, yet the value of the local \mathcal{R} function is small ($R\mathcal{R}^{\text{loc}} = 0.78$ fm), indicating that local levels are either distant or rather evenly balanced between bound and unbound.

It is of more concern that the measured cross sections are almost always lower than the calculated direct capture. The average factor of discrepancy is 0.65 for the [$G + V$] values and 0.60 for the [S] values. A possible mechanism for causing such a systematic effect is the influence of collective motion. The low-lying-level spectrum of ^{44}Ca resembles that expected for a spherical nucleus soft to vibrations. We now outline briefly the way in which such vibrational motion of the "core" potential can affect the capture of a single neutron.

IV. EFFECT OF COLLECTIVE MOTION ON DIRECT CAPTURE

The potential field provided by the target for the impinging neutron is deformed dynamically from the equilibrium spherical shape. The potential can be represented as an expansion in harmonic multipoles. The zeroth-order term, which can be considered as an overall average spherical field, can be incorporated into a spherical

single-particle Hamiltonian. With spin-orbit coupling of the usual form this term generates a relatively normal shell-model sequence of single-particle states and, if incorporated into an optical model, fairly typical s -wave scattering behavior. To form a system of nuclear states that are available for excitation by the incoming neutron, the collective states of the target are coupled to scattering states (real or virtual) of higher orbital angular momentum. The basis states thus formed are mixed by including the higher multipole terms of the expansion of the deformed potential in the Hamiltonian, and the wave function can be calculated by coupled-channel methods. Because of the higher multipole mixing, the s -wave scattering amplitude is modified, causing a corresponding change in the potential-capture amplitude and virtual excitation of collective states of the target occurs accompanied by finite amplitudes of the neutron wave function in closed channels of higher orbital angular momentum; these last wave functions attenuate to zero with increasing radial separation of the neutron and target. The same higher multipole terms will likewise cause mixing between lower states consisting of bound, unfilled single-particle orbitals coupled to the ground state and collective motions of the target, respectively. Thus, in the case of a quadrupole mixing potential, for example, electric-dipole matrix elements for the s -wave elastic-scattering state to a final p -wave single-particle state (the target nucleus ground state remaining unchanged) will be accompanied by contributions from a d -wave single-particle state to a component in the final state or p -wave or f -wave single-particle nature coupled to an unchanged collective motion of quadrupole character.

The first 2^+ state of ^{44}Ca is at 1.16 MeV (followed by the sequence 0^+ at 1.88 MeV, 4^+ at 2.28 MeV, and 2^+ at 2.66 MeV). We ignore the higher states and treat only the states of ^{45}Ca formed by including the ground state (zero phonon) and the first-excited state (one phonon) in the wave functions. The restoring force constant for the harmonic-oscillator wave functions of these two states of ^{44}Ca is taken from the surface energy for incompressible nuclear fluid, $4\pi R_0^2 S = 17 A^{2/3} \text{ MeV}$. The basis states that we consider for the capture transitions in ^{45}Ca are the products of a single-particle neutron state with one of the above two vibrational states of the core ^{44}Ca . For final states of total angular momentum $J_f^\pi = \frac{3}{2}^-$ in ^{45}Ca , the basis states are thus of form $2p_{3/2} \otimes 0^+$, $1f_{7/2} \otimes 2^+$, $2p_{3/2} \otimes 2^+$, and $2p_{1/2} \otimes 2^+$. For final states $J_f^\pi = \frac{1}{2}^-$, the basis states are $2p_{1/2} \otimes 0^+$ and $2p_{3/2} \otimes 2^+$. We describe the initial state (angular momentum $J^\pi = \frac{1}{2}^+$) in terms of discrete R -matrix states, and the principal basis states we consider are $3s_{1/2} \otimes 0^+$, $2d_{5/2} \otimes 2^+$, and $2d_{3/2} \otimes 2^+$, but the other principal quantum numbers up to $5s$ and $4d$ are included in the diagonalization. We assume that the potential radius has the form

$$R(\theta, \phi) = R_0 [1 + \beta \cos \gamma Y_{20} + \beta \sin \gamma (Y_{22} + Y_{2-2}) / \sqrt{2}], \quad (9)$$

where β and γ are the instantaneous deformation parameters; the $Y_{\lambda\mu}$ are spherical harmonics with arguments θ, ϕ that are spherical polar angles of the radius vector in

the body-centered coordinate frame of the nucleus; and the zeroth-order (spherical) term of the potential is just the Woods-Saxon form with radius R_0 given by $(1.16A^{1/3} + 0.6)$ fm. Then, the quadrupole potential coupling term is

$$V_2 = \frac{R_0[\beta \cos\gamma Y_{20} + \beta \sin\gamma(Y_{22} + Y_{2-2})]}{\{1 + \exp[(r - R_0)/d]\}^2 d} \\ \times V_0 \exp[(r - R_0)/d]. \quad (10)$$

This term is to be integrated over β, γ as well as r, θ, ϕ , in forming the matrix elements of the basis states. The calculations are described in more detail in the Appendix.

The salient conclusions from these calculations, made for the $J = \frac{3}{2}$ final states, are the following.

(i) The "simple" direct-capture cross section (i.e., that from the transition amplitude for $s_{1/2} \otimes 0 \rightarrow p_{3/2} \otimes 0$) is approximately the value that would be calculated using the coherent scattering length and final-state spectroscopic factor within the spherical optical-model theory.

(ii) There is considerable mixing of configurations in the final states, with the main effect that the amplitudes of the $2p_{3/2} \otimes 0$ component on the one hand and either the $1f_{7/2} \otimes 2$ or $2p_{3/2} \otimes 2$ component (whichever is dominant) on the other in the two lowest final states have opposite phase, whereas the corresponding important amplitudes in the two higher states have the same phase.

(iii) The mixing of the important R -matrix eigenfunctions describing the initial state is also quite strong, with a negative relative phase effect between the $3s_{1/2} \otimes 0$ and $2d_{5/2, 3/2} \otimes 2$ components.

(iv) For the mixed states the transition amplitudes for the $2d_{5/2} \otimes 2 \rightarrow 2p_{3/2} \otimes 2$ and $2d_{5/2} \otimes 2 \rightarrow 1f_{7/2} \otimes 2$ components are not insignificant compared with the "direct" term, $s_{1/2} \otimes 0 \rightarrow p_{3/2} \otimes 0$, and the relative phases of the admixtures (as described above) are such that the interference is destructive for the two lowest final states and constructive for the higher states. These effects result in cross sections that are reduced to less than or about one-half of the direct-capture estimate for the lower states, and approximately doubled for the higher states.

(v) Because 62% of the $2p_{3/2} \otimes 0$ state is included in the two lower states, we can still expect, even after allowing for further mixing through other residual forces, that the bulk of the higher-energy gamma-ray transitions, which are the ones most prominent in the spectrum through both the E_γ^3 phase-space factor and normal experimental bias, will be dominated by the properties of these two states rather than the upper two. Thus we can expect, in qualitative agreement with the observations, that there will be a systematic bias towards low values of the capture cross sections in comparison with the predictions of the direct-capture model.

We have thus demonstrated the plausibility of the hypothesis that the rather systematic discrepancy between the spherical optical-model estimates and the experimental data is due to the softness of the ^{44}Ca target nucleus, allowing virtual excitation of quadrupole collective vibrations with amplitude sufficient to add interfering contributions to the direct radiative capture amplitude. We

stress, however, that the capture cross section in this coupled-channel model cannot be calculated as precisely, and in as parameter-free a manner, as is possible for the rigid spherical optical model. Critical factors affecting calculations in the coupled-channel model are the value of the restoring force constant, the spacing of the single-particle orbitals of different orbital angular momentum, and the assumption that the correlation between the amplitudes of the coupled-channel configurations in the final states will not be significantly upset by additional mixing forces not taken into account here.

V. CONCLUSIONS

The contribution of the experimental work described in this paper has been to produce a much more complete and accurate set of coherent neutron scattering lengths for the stable isotopes of calcium. These were needed in the first place to refine the analysis of thermal-neutron capture data on primary gamma-ray transitions of these isotopes. We have carried out this analysis with the improved scattering-length data.

Many of the general conclusions of Ref. 1 are unchanged as a result of the current analysis. Thermal-neutron capture by ^{40}Ca , ^{42}Ca , and ^{48}Ca is confirmed to be controlled largely by the direct mechanism. In the case of ^{42}Ca , this is now a definitive result; in fact, this is one of the purest cases of direct thermal-neutron capture yet observed, with very little admixture of compound-nucleus component apparent. For ^{40}Ca the compound-nucleus component appears to be about an order of magnitude greater, but it is still a minor component of the picture and can be accounted for by postulating a quite normal (bound) local level. There are only two significant transitions following thermal-neutron capture by ^{48}Ca . These are to final states that are of almost pure single-particle nature. The cross section for one is explained well by the direct-capture theory, but the other differs by three standard deviations; it is not possible to be certain that the discrepancy is significant.

The new value of the coherent scattering length of ^{44}Ca disturbs the tentative conclusions drawn in Ref. 1 that capture by this nucleus too can be attributed to optical-model direct capture with a relatively modest contaminant from the compound nucleus. It now appears that the measured cross sections for the transitions are substantially lower than the theoretical values on average. We have noted, however, that ^{44}Ca , occurring midway between the $N=20$ and 28 shells, appears to have the character of a spherical vibrator, and the coupling of single-particle states by this collective motion could well account for the lower cross sections found for the bulk of the gamma rays in the 4- to 6-MeV range.

ACKNOWLEDGMENTS

E.L. wishes to express his deep appreciation for the generous hospitality afforded by the Argonne National Laboratory and The University of Chicago. The authors thank Jack Harvey for a critical reading of the manuscript. The current research was sponsored in part

by the U.S. Department of Energy under Contract No. DE-AC05-84OR21400 with Martin Marietta Energy Systems, Inc. (Oak Ridge), Contract No. W-7405-Eng-82 with the Iowa State University (Ames) and Contract No. W-31-109-Eng-38 with the University of Chicago (Argonne). One of the authors (E.L.) was also supported by the Underlying Research Program of the United Kingdom Atomic Energy Authority.

APPENDIX

Here we discuss in more detail the nature of the calculations on the effect of collective coupling in modifying the direct-capture model. These calculations are based on the matrix elements of the coupling term, Eq. (10). This term is to be integrated over β, γ as well as r, θ, ϕ , in forming the matrix elements of the basis states.

The values of the matrix elements for the final states of $J_f^{\pi} = \frac{3}{2}^-$ range from 1.1 MeV (connecting the $2p_{3/2} \otimes 0^+$ and $1f_{7/2} \otimes 2^+$ states) to 1.8 MeV ($2p_{3/2} \otimes 0^+$ and $2p_{3/2} \otimes 2^+$ states). The single-particle components of the basis states have been computed for a binding energy of 5 MeV; i.e., the potential well depth was adjusted to determine the wave function with this eigenvalue. Thus the radiation widths computed for transitions to these states are for typical gamma rays of about 5 MeV energy. The eigenvalues E_m of the basis states m have been taken as the sum of the core state (0 or 1.16 MeV) and the single-particle state. The values of the latter have been guided by the spectroscopic information on ^{43}Ca . In this nucleus the $p_{3/2}$ state is bound by 5.8 MeV, the $f_{7/2}$ state is at -8 MeV, and the $p_{1/2}$ state is calculated to lie 2.5 MeV above the $p_{3/2}$ state. The diagonalized states have eigenvalues E_μ separated by about 3 MeV for the two lowest states, while the others are at 1.5 and 3.7 MeV above the second lowest state. We find that 62% of the $2p_{3/2} \otimes 0^+$ state is included in the lowest two states. Even after allowing for further mixing through other residual forces, we can still expect that the bulk of the higher-energy gamma-ray transitions, which are the ones most prominent in the spectrum through both the E_γ^3 factor and normal experimental bias, will be dominated by the properties of these two states rather than the upper two.

The initial state for the capture transition can be described in terms of R -matrix discrete eigenstates constructed for the coupled-channel optical-model scattering problem. We shall construct these in the first place for a real potential well. The basis states are denoted with subscript n ; their eigenvalues are E_n , and radial wave functions u_n . Those basis states that contain the zero-phonon core are calculated with a boundary condition appropriate for a low-energy s -wave neutron at the channel radius (which is taken as $R_0 + 7d$). Those with the one-phonon core are calculated with the boundary condition of d -wave neutrons bound by 1.16 MeV. The potential well for the single-particle states has the Moldauer¹⁶ global optical-model parameters. The matrix elements for the R -matrix basis states have values of the order of 0.6 to 0.9 MeV for the principal collective couplings $3s_{1/2} \otimes 0^+$ to $2d_{5/2} \otimes 2^+$ and $3s_{1/2} \otimes 0^+$ to $2d_{3/2} \otimes 2^+$. Their entrance channel amplitudes at the channel radius (which are

nonzero only for the $s_{1/2} \otimes 0^+$ states), and the radiative width amplitudes to the various components of the final states E_μ can be computed for the spherical component of the potential well. The most important R -matrix state governing low-energy scattering, the $3s_{1/2} \otimes 0^+$ state at 0.714 MeV, has entrance channel amplitude $u_n(R_c) = 1.667(10^{-12} \text{ cm})^{1/2}$ and radiative width amplitude (to the lowest final state E_μ) of $\Gamma_{n(\gamma \rightarrow p_{3/2} \otimes 0^+)}^{1/2} = 0.0103 \text{ MeV}^{1/2}$. The nearby $2d_{5/2} \otimes 2^+$ and $2d_{3/2} \otimes 2^+$ states have radiation width amplitudes of $\Gamma_{n(\gamma \rightarrow f_{7/2} \otimes 2^+)}^{1/2} = -0.0082 \text{ MeV}^{1/2}$, $\Gamma_{n(\gamma \rightarrow p_{3/2} \otimes 2^+)}^{1/2} = -0.0019 \text{ MeV}^{1/2}$, and $\Gamma_{n(\gamma \rightarrow p_{3/2} \otimes 2^+)}^{1/2} = -0.0019 \text{ MeV}^{1/2}$, $\Gamma_{n(\gamma \rightarrow p_{1/2} \otimes 2^+)}^{1/2} = -0.0011 \text{ MeV}^{1/2}$, respectively. From these the R function for scattering and the corresponding radiative transition amplitude (excluding the hard-sphere contribution from the channel radius) can be computed for a real well with no collective mixing. For this uncoupled case (UC) the \mathcal{R} -matrix element and capture amplitude due to the R -matrix levels are

$$\mathcal{R}^{(\text{UC})} = \sum_n \gamma_n^2 / (E_n - E), \quad (\text{A1})$$

$$\gamma_n^{(\text{UC})2} = (\hbar^2 / 2MR_0) u_n^2(R_c), \quad (\text{A2})$$

$$U_{\gamma \rightarrow \mu}^{(\text{UC})} = \sum_m U_{[\gamma \rightarrow \mu(m)]}^{(\text{UC})}, \quad (\text{A3})$$

and

$$U_{\gamma \rightarrow \mu(m)}^{(\text{UC})} = \sqrt{2P_0} \sum_n \gamma_n \Gamma_{n[\gamma \rightarrow \mu(m)]}^{1/2} / (E_n - E), \quad (\text{A4})$$

where $\Gamma_{n[\gamma \rightarrow \mu(m)]}^{1/2}$ is the radiation width amplitude for a transition from the R -matrix level n to a given basis component m (in this case the $2p_{3/2} \otimes 0$ or $2p_{1/2} \otimes 0$ configuration) in the final state μ , M is the reduced mass of neutron and target, and P_0 is the s -wave neutron penetration factor. In addition to the term $U_{\gamma \rightarrow \mu}^{(\text{UC})}$, there is a hard-sphere capture amplitude $U_{\gamma \rightarrow \mu}^{\text{HS}}$ connecting an initial-state component proportional to $\sin[k(r - a_0)]$ in the external region with the $2p_{1/2} \otimes 0^+$ component of the final state. In the present case we find $\mathcal{R}^{(\text{UC})} = 1.01$ for the channel radius $R_c = 9.035 \text{ fm}$ and $U_{\gamma}^{(\text{UC})} = U_{\gamma} - U_{\gamma}^{\text{HS}} = 1.6 \times 10^{-4}$ for the lowest final state E_μ . A separate calculation gives for the hard-sphere contribution $U_{\gamma}^{\text{HS}} = -1.5 \times 10^{-5}$. Comparison of these results with the calculations from the usual optical-model code (with zero imaginary component) yields correction terms that allow for the effect of higher R -matrix states ($6s_{1/2}$ and above) that have not been included explicitly in the R -matrix calculation. The correction to $\mathcal{R}^{(\text{UC})}$ is 0.035 and that to $U_{\gamma}^{(\text{UC})}$ is 2.9×10^{-5} . The scattering and potential-capture cross sections are

$$\sigma_{\text{sc}} = 4\pi R_c^2 (1 - \mathcal{R}^{(\text{UC})})^2 \quad (\text{A5})$$

and

$$\sigma_{\text{pot}, \gamma} = \pi (U_{\gamma}^{(\text{UC})} + U_{\gamma}^{\text{HS}})^2 \mathcal{W} / k^2, \quad (\text{A6})$$

where \mathcal{W} is the spin-coupling factor.²

The diagonalized R -matrix states E_ν can be computed

from the basis states and their matrix elements. From the state amplitudes $c_{\nu n}$ and the entrance channel and radiative width amplitudes of the basis states, we can calculate the entrance channel amplitudes and radiative width amplitudes of the E_ν to the various components of the final state. The most important R -matrix state is found at $E_\nu=0.323$ MeV; its main component has amplitude $c_{\nu n}=0.94$ (where n here denotes $3s_{1/2}\otimes 0^+$), while significant admixtures come from the $2d_{5/2}\otimes 2^+$ ($c_{\nu n'}=-0.31$) and $2d_{3/2}\otimes 2^+$ ($c_{\nu n''}=0.13$) basis states. Other important R -matrix states are 3.24 MeV (88% $2d_{5/2}\otimes 2^+$) and 5.39 MeV (96% $2d_{3/2}\otimes 2^+$). The R -matrix element for the coupled case is

$$\mathcal{R}^{(c)} = \sum_{\nu} \gamma_{\nu}^2 / (E_{\nu} - E), \quad (\text{A7})$$

where the reduced s -wave neutron widths are

$$\gamma_{\nu}^2 = (\hbar^2 / 2MR_c) \left[\sum_n c_{\nu n} u_n(R_c) \right]^2. \quad (\text{A8})$$

The principal term in the capture amplitude is

$$U_{\gamma \rightarrow \mu}^{(c)} = \sqrt{2P_0} \sum_{\nu} \gamma_{\nu} \Gamma_{\nu(\gamma \rightarrow \mu)}^{1/2} / (E_{\nu} - E), \quad (\text{A9})$$

where

$$\Gamma_{\nu(\gamma \rightarrow \mu)}^{1/2} = \sum_m c_{\mu m} \sum_n c_{\nu n} \Gamma_{n(\gamma \rightarrow m)}^{1/2}. \quad (\text{A10})$$

Thus $U_{\gamma \rightarrow \mu}^{(c)}$ can be rewritten as

$$U_{\gamma \rightarrow \mu}^{(c)} = \sum_m U_{\gamma \rightarrow \mu(m)}^{(c)}, \quad (\text{A11})$$

where

$$U_{\gamma \rightarrow \mu(m)}^{(c)} = \sqrt{2P_0} \sum_{\nu} \gamma_{\nu} \sum_n c_{\nu n} \Gamma_{n[\gamma \rightarrow \mu(m)]}^{1/2} / (E_{\nu} - E), \quad (\text{A12})$$

and

$$\Gamma_{n[\gamma \rightarrow \mu(m)]}^{1/2} = c_{\mu m} \Gamma_{n(\gamma \rightarrow m)}^{1/2}. \quad (\text{A13})$$

The value for $\mathcal{R}^{(c)}$ is 1.75 (including the same correction term as in the unmixed case). The value of the capture amplitude to only the $2p_{3/2}\otimes 0^+$ component of the final state is -3.5×10^{-4} (including the hard-sphere component). The capture cross section resulting from this is less than 15% different from the value obtained from an optical-model calculation with real potential adjusted to reproduce the new potential scattering section. If the transitions to the remaining components of the final state are now included in the capture amplitude, we find that the capture cross section is reduced to about one-quarter of the value calculated from the optical model. A similar effect is observed when the previous computations are repeated for the next lowest state. In this case when the effect of collective coupling is included, the full capture cross section is about 40% of the spherical optical-model value. On the other hand, the cross sections to the upper two final states (the effects of which are expected to be much less apparent in the capture gamma-ray spectrum) are found to be about twice the optical-model values.

Although these results are indicative and appear to give a semiquantitative explanation of the deviation be-

tween experiment and direct-capture theory in the case of ^{44}Ca , a more realistic model will include the effect of damping due to other residual forces in the Hamiltonian; these are expected to contribute the bulk of the imaginary potential term in the spherical optical model. This effect can be included in the R -matrix theory used above by allowing dissolution of the single-particle strength of the R -matrix levels among the denser background of compound-nucleus states (which we still describe in R -matrix form). Only the contributions to the reaction amplitudes from the state closest to zero energy will be significantly affected by such spreading. For this nearest level, ν , the R function is now

$$\mathcal{R}_{\nu} = \gamma_{\nu}^2 \left[\frac{E_{\nu}}{E_{\nu}^2 + W_{\nu}^2} \right], \quad (\text{A14})$$

where $\gamma_{\nu}^2 = (\hbar^2 / 2MR_c) \mu_{\nu}(R_c)$ is the reduced neutron width of the undamped state ν and W_{ν} is the spreading width of this state. We estimate the latter as follows. We determine the value of $\mathcal{R}^{(\text{UC})}$ in the uncoupled case (UC) from the optical model with the peak value of the imaginary potential restored to its original value of -15 MeV. We find $\mathcal{R}^{(\text{UC})} = 0.744$. If we remove the contribution of all the levels, except the $3s_{1/2}\otimes 0$ at 0.714 MeV, from this, we have the optical model estimate of $\mathcal{R}_{\nu}^{(\text{UC})} = 0.673$. Substituting in Eq. (A14) we find $W_{\nu} = 0.425$ MeV. We now use this result in Eq. (A14) for the 0.323-MeV level of the collective coupling case (c) and find $\mathcal{R}_{\nu}^{(c)} = 0.576$. Adding to this the contribution from all the other levels (undamped to good approximation), we find $\mathcal{R}^{(c)} = 0.72$, i.e., the value of the potential scattering length is almost unchanged from that of the uncoupled case.

We use the same procedure to modify the capture amplitudes for the effect of damping. The contribution to the capture amplitude from the state ν is, with damping,

$$U_{\nu, \gamma} = \left[\frac{\hbar^2 k}{M} \right]^{1/2} \frac{u_{\nu}(R_c) \Gamma_{\nu}^{1/2} E_{\nu}}{E_{\nu}^2 + W_{\nu}^2}. \quad (\text{A15})$$

Application of this contribution to the uncoupled states give $U_{\gamma}^{(\text{UC})} = -1.19 \times 10^{-4}$ (cf. -1.63×10^{-4} for $W_{\nu} = 0$). With the addition of the hard sphere component, this leads to a value of the potential-capture cross section, $\sigma_{\text{pot}, \gamma} = 0.46$ mb, in close agreement with optical-model calculation (0.48 mb). For the coupled states the potential-capture cross section is 35% of this value. Inclusion of the valence term does not alter qualitatively this reduction effect of the collective motion. The radiation with amplitude of the $E_{\nu} = 0.32$ MeV level is $-1.96 \times 10^{-3} \text{ MeV}^{-3}$ to the lowest final state (inclusive of all components). For the uncoupled $E_n = 0.714$ MeV state, it is $-5.84 \times 10^{-3} \text{ MeV}^{-3}$. The ratio of the reduced neutron width amplitudes is 0.88. Substitution of these changes in the estimate of the direct-capture cross section leads to a value that is about one-third of that calculated by the $(G+V)$ method. Therefore, the inclusion of damping does not qualitatively modify the previous conclusion that the coupling induced by the collective vibrational states of ^{44}Ca has a significant effect in reducing the direct-capture cross section to the most important components of the final states of ^{45}Ca .

- *Permanent address: Nuclear Research Centre-Negev, Beer Sheva, Israel.
- †Permanent address: UK Atomic Energy Agency, Harwell, England.
- ¹S. Kahane, J. E. Lynn, and S. Raman, *Phys. Rev. C* **36**, 533 (1987).
- ²S. Raman, R. F. Carlton, J. C. Wells, E. T. Journey, and J. E. Lynn, *Phys. Rev. C* **32**, 18 (1985).
- ³J. E. Lynn, S. Kahane, and S. Raman, *Phys. Rev. C* **35**, 26 (1987).
- ⁴A. M. Lane and J. E. Lynn, *Nucl. Phys.* **17**, 563 (1960); **17**, 586 (1960).
- ⁵A. M. Lane and S. F. Mughabghab, *Phys. Rev. C* **10**, 412 (1974).
- ⁶J. Cugnon and C. Mahaux, *Ann. Phys. (N.Y.)* **94**, 128 (1975).
- ⁷C. G. Shull and E. O. Wollan, *Phys. Rev.* **81**, 527 (1951).
- ⁸M. Atogi, *J. Chem. Phys.* **35**, 61 (1950).
- ⁹A. Kvik, K. Stahl, and J. V. Smith, *Z. Krist.* **171**, 141 (1985).
- ¹⁰L. Koester, in *Neutron Physics*, Vol. 80 of *Springer Tracts in Modern Physics* (Springer-Verlag, Berlin, 1977), p. 36.
- ¹¹L. Koester (private communication).
- ¹²J. W. Richardson, Jr. (private communication).
- ¹³R. W. G. Wyckoff, *Crystal Structures* (Interscience, New York, 1967), Vol. 2, p. 367.
- ¹⁴H. M. Rietveld, *J. Appl. Cryst.* **2**, 65 (1969).
- ¹⁵H. Effenberger, K. Mereiter, and J. Zemann, *Z. Krist.* **156**, 223 (1981).
- ¹⁶P. A. Moldauer, *Nucl. Phys.* **47**, 65 (1963).
- ¹⁷A. G. W. Cameron, *Can. J. Phys.* **37**, 322 (1959).
- ¹⁸S. F. Mughabghab, M. Divadeenam, and N. E. Holden, *Neutron Cross Sections* (Academic, New York, 1981), Part A, p. 5.